www.crt-journal.org

CRYSTAL Research & Technology

WILEY-VCH

CRYSTAL Research & Technology

Cryst. Res. Technol. **49**, No. 9, 736–742 (2014) / DOI 10.1002/crat.201400102

Original Paper

Effect of Mn doping on the growth and properties of enstatite single crystals

Manuela Catalano[1], Andrea Bloise[1,], Valentino Pingitore[2], Domenico Miriello[1], Enzo Cazzanelli[2], Marco Giarola[3], Gino Mariotto[3], and Eugenio Barrese[1]*

Received 28 March 2014, revised 25 June 2014, accepted 21 July 2014
Published online 21 August 2014

Millimetric Mn-doped enstatite ($MgSiO_3$) crystals have been grown by slow cooling in MoO_3, V_2O_5, and Li_2CO_3 flux. Six starting mixture with different amount of manganese were slowly cooled from 1350 °C, 1050 °C and 950 °C down to 750 °C, 650 °C and 600 °C respectively. The enstatite crystals were characterized by X-ray powder diffraction (XRPD) and scanning electron microscopy with energy-dispersive spectrometry (SEM/EDS). Mn-doped enstatite crystals were reddish in color, euhedral and elongate parallel to c-axis. The largest enstatite crystal obtained is 8.5 mm in length. The effects of growth parameters on yield and size of crystals were studied. Variations observed in crystal size were attributed to the amount of Mn doping. Further characterizations by μ-Raman spectroscopy (μ-R) and cathodoluminescence (CL) allowed to study the effect of Mn doping on some chemical/physical characteristics of the enstatite and to assess its potential in advanced technological applications.

1 Introduction

Enstatite ($MgSiO_3$), the Mg-end member of the pyroxene silicate family is of well-known scientific and technological interest being ideal substrate in electronics and optimal material for thermal insulation in applications at high temperatures [1–4]. Recently, silicates built on silica tetrahedron have been investigated and suggested as suitable dielectric materials for millimeter wave communication [5].

Over the last few decades, numerous investigations have been carried out to evaluate the possible changes of the main properties of enstatite when synthetic crystals are doped with various cations. So far enstatite was doped with several amounts of Eu^{2+}, Dy^{3+}, Cr^{3+}, Li^{+}, Sc^{3+} Ni^{2+} and Ti^{4+} [6–9] mainly to study the luminescence behaviour of so doped materials. Lately, it was reported that manganese used as dopant improves the microwave dielectric properties of silicates [10]. Furthermore, it has been shown that enstatite crystals doped with transition metals (e.g., Mn^{2+}), can be considered good long-lasting phosphors for various applications such as emergency lighting, safety indication and road signs because of their resistance to acid and alkali [11, 12].

To date, synthesis of Mn-doped enstatite crystals and the effects of this dopant on the growth and some properties of them has only be studied by a few authors. Ito (1975) [13] reported a tentative of growth of Mn-enstatite by flux method, but without defining in detail the influence of the Mn-dopant on its growth, while, in other works [11, 12], researchers focused the attention mainly on luminescent properties of some nanometric Mn-doped crystals obtained using sol-gel method.

The aim of this work is to grow enstatite by slow cooling flux method in order to obtain large single crystals and to study how some chemical and physical characteristics of them change by varying the amount of manganese content. The slow cooling flux method was preferred to other methods (e.g., sol-gel) because of the possibility to obtain large single crystals useful for the evaluation of the quality of the crystals obtained (e.g., crystallinity, uniformity, purity etc.).

2 Experimental

2.1 Procedures for single crystal growth

In order to obtain Mn-doped enstatite, the following starting materials were used: granular quartz (SiO_2; Carlo

* Corresponding author: e-mail: andrea.bloise@unical.it
[1] Department of Biology, Ecology and Earth Sciences, University of Calabria, 87036 Rende, Italy
[2] Department of Physics, University of Calabria, 87036 Rende, Italy
[3] Department of Computer Science, University of Verona, 37134 Verona, Italy

CRYSTAL Research&Technology

Table 1 Molar ratios of starting nutrient mixtures, experimental conditions and products obtained.

Run	Nutrient (molar ratio)			Starting cooling T (°C)	Cooling rate (°C/h)	Cut off temperature (°C)	Minerals produced	Average MnO in enstatite (wt.%)	Max length enstatite (mm)	Average length enstatite (mm)	Chemical formula of Mn-doped enstatite
	MgO	SiO_2	MnO								
H1	1.00	1.00		1350	3.7	750	Mg-En>Qtz				
EN1	0.50	1.00	0.50	1350	3.7	750	Mn-En>Qtz	8.87	5.0	2.6	$Mg_{0.86}Mn_{0.14}SiO_3$
EN2	0.75	1.00	0.25	1350	3.7	750	Mn-En>Qtz	6.35	8.0	3.8	$Mg_{0.91}Mn_{0.09}SiO_3$
EN3	0.60	1.00	0.40	950	2.1	600	Mn-En>Qtz	6.30	7.0	3.4	$Mg_{0.89}Mn_{0.11}SiO_3$
EN4	0.25	1.00	0.75	950	2.1	600	Br>Qtz				
EN5	0.00	1.00	1.00	950	2.1	600	Qtz>Br				
EN6	0.50	1.00	0.50	1050	1.7	650	Mn-En>Qtz	8.56	5.0	3.3	$Mg_{0.87}Mn_{0.13}SiO_3$
EN7	0.60	1.00	0.40	1050	1.7	650	Mn-En>Qtz	6.28	8.5	4.4	$Mg_{0.90}Mn_{0.10}SiO_3$
EN8	0.40	1.00	0.60	1050	1.7	650	Mn-En>Qtz	9.89	3.0	1.8	$Mg_{0.80}Mn_{0.20}SiO_3$
EN9	0.00	1.00	1.00	1050	1.7	650	Br>Qtz				

Mg-En = Undoped enstatite; Mn-En = Mn-doped enstatite; Qtz = quartz, Br = braunite

Erba reagent, code No. 364011), magnesium oxide (MgO; Carlo Erba reagent, code No. 459586) and manganese oxide (MnO; Aldrich reagent, code No. 8849). To increase the reactivity between starting materials, as seen in previous experiments [9], each starting material was pretreated as follows: granular quartz was converted into cristobalite by heating powdered SiO_2 to 1400 °C; MgO powder was converted into periclase by heating to 900 °C; MnO was heated to 110 °C for several hours in order to eliminate its hygroscopicity. Cristobalite (SiO_2), periclase (MgO) and manganese oxide (MnO) powders with different molar ratio (Table 1) were loaded in 50 ml platinum crucible and placed inside a vertical furnace equipped with Super Kanthal heating element (0 °C – 1700 °C). The addition of lithium-vanadomolybdate flux [14–17] was performed to the starting materials with a constant starting materials/flux ratio of 0.5.

The growth condition of enstatite is restricted at a range of temperature estimated from phase diagrams reported by Ito (1982) [16] and Tanaka & Takei (1997) [18]. The mixtures were first brought to 1350 °C, 1050 °C and 950 °C in an oxidizing atmosphere and kept at these temperatures for about 100 h for more homogenization. Then, they were slowly cooled down to 750 °C, 600 °C and 650 °C with three different cooling rate (3.7 °C/h, 2.1 °C/h and 1.7 °C/h). Finally, the crucibles were rapidly quenched down to room temperature by immersion in water. The composition of the grown mixtures, conditions of synthesis and final products are listed in Table 1. Undoped enstatite ($MgSiO_3$), synthesized to be compared with the Mn-doped one was also reported in Table 1 (run H1).

2.2 Characterization techniques

After the separation from the solidified flux by sonication in hot water, doped enstatite crystals were recovered under a binocular microscope (20x), selected and then characterized by a X-ray powder diffractometer (XRPD; Bruker D8 Advance) with Cu-Kα radiation, operating at 40 kV and 40 mA. Scans were collected on powder samples in the range of 3–60° 2θ, step interval 0.02° 2θ, step-counting time 3 s. The chemical composition and morphology of the crystals were investigated by energy dispersive spectroscopy (EDS) with a field-emission scanning electron microscope (SEM, FEI Quanta 200).

The micro-Raman (μ-R) measurements were carried in the usual backscattering geometry by means of a triple monochromator (Horiba-Jobin Yvon, model T 64000), equipped with holographic gratings having 1800 lines/mm, and set in double subtractive/single configuration. The spectra were excited by the 514.5 nm line of a mixed Ar-Kr gas laser. The laser beam was focused onto a spot of ~5 μm in size through the lens

of a 10X microscope objective with numerical aperture N.A. = 0.25.

After the filtering by the double monochromator, the scattered radiation was detected at the spectrometer output by a multichannel charge coupled-device detector (CCD), with 1024 × 256 pixels, cooled by liquid nitrogen. The high spectral dispersion of this apparatus provides a good resolution of the collected spectra, necessary for a better estimation of peak frequency and linewidth, i.e. one spectral point for 0.2 cm^{-1}. In addition, spectral lamp emission lines were used to check the frequency calibration of the instrument. Cathodoluminescence (CL) measurements have been performed using a Cambridge Stereoscan 360 SEM, equipped with a Horiba Jobin Yvon VS140 UV-VIS spectrometer with a spectral resolution of ~ 1 nm. The SEM operating conditions were: 20–40 kV of accelerating voltage, 1 μA for the emission current, 12.5 Hz for the scannning frequency, an acquisition time of 40s and a scanning area ranging from 0,1 to 0,4 mm^2 . Our interest has been focused on qualitative spectral changes at room temperature.

3 Results and discussion

The formation of products from the solidified flux during the cooling was hindered and the quench material contained, besides Mn-doped enstatite and quartz, only lithium silicon oxide ($Li_2Si_2O_5$; JCPDS No. 04–0436). Quenched solute from the flux appeared as grey/reddish, soft material that could easily be removed from the crystals surface. All Mn-doped enstatite crystals are reddish in color (figure 1). The color intensifies progressively with increasing amount of manganese in the crystals. A visual inspection by means of binocular microscopes shows that run products consisted of approximately 90% Mn-doped enstatite crystals and 10% quartz. The abundance of Mn-doped enstatite was nearly the same in all runs. Almost all enstatite appears to be idiomorphic forming long prismatic (figure 1a) and short prismatic (figure 1b) crystals commonly without defects. The largest crystal measured 8.5 mm in length, while the smallest one was few microns. Inspection of the recovered enstatite crystals revealed that they were inclusions-free. In some rare specimens, veins occurred, which contain some quenched material. XRPD analyses acquired on all runs showed the presence of both ortho- and clino-enstatite.

The diffraction peaks were found to match with the JCPDS standard (No. 19-0768) data of enstatite-type orthorhombic structure and with the JCPDS standard (No. 03-0521) data of enstatite clino-type. The diffraction

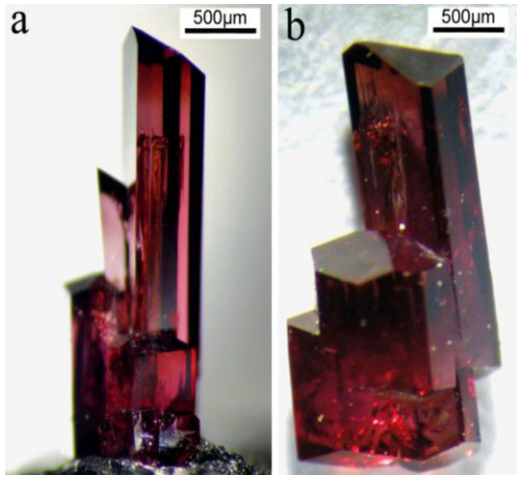

Fig. 1 Optical image of reddish crystals of Mn-doped enstatite a) long prismatic enstatite, run EN1; b) short prismatic enstatite, run EN7.

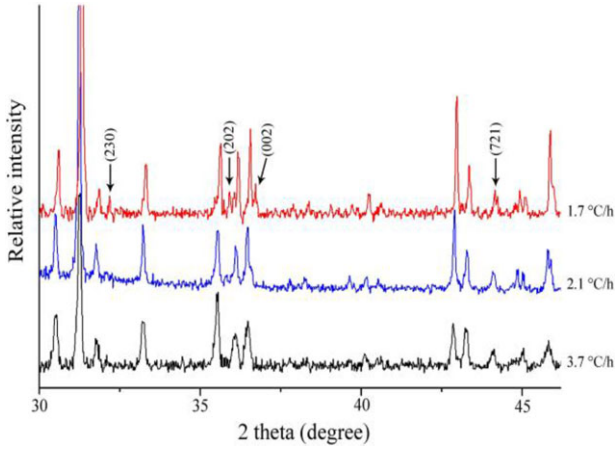

Fig. 2 XRPD spectra of Mn-doped enstatite grown at different cooling rate. Black line: run EN1; blue line: run EN3; red line: run EN7. Arrows indicate new reflection peaks in the XRPD patterns of Mn-doped enstatite.

peaks are observed to be slightly shifting towards lower angles with increasing Mn content which indicate that Mn^{2+} ion has substituted the Mg^{2+} in octahedral site.

Figure 2 illustrates the XRPD patterns of Mn-doped enstatite growth at three different cooling rate. It can be inferred from the patterns (figure 2) that cooling rate plays a key role in the formation of crystals with high crystallinity. Indeed, the results indicate that the sharpness of the peaks, which represents the crystallinity degree of the materials, decreases with increasing of cooling rate at which crystals were grown. This is reflected, for example, by the evolution of the full width at half-maximum

CRYSTAL Research&Technology

(FWHM) of the main reflection at (6 1 0): FWHM value increases from 0.068° to 0.077° and to 0.147° when cooling rate increases from 1.7 °C/h to 2.1 °C/h and to 3.7 °C/h respectively. Moreover, the appearance of new reflection peaks in the XRPD pattern of Mn-doped enstatite grown at 1.7 °C/h confirms the higher crystallinity of this sample respect to the other ones.

The formation of clinoenstatite by quenching at 600 °C and higher temperatures was probably due to shearing orthoenstatite [18–20]. Fast cooling cannot be invoked as a consequence of the growth of clinoenstatite [21] because it was also found in the run with slower cooling rate (i.e., 1.7 °C/h, Table 1).

XRPD and EDS/SEM analyses of all products obtained confirm that quartz was also found in all runs in addition to Mn-doped enstatite (Table 1). When moderate amounts of MnO were present in the starting mixture, manganese did not impede the growth of Mn-doped enstatite. However, when the MnO (molar ratio) was ≥ 0.75 (run EN4, EN5, EN9), Mn-doped enstatite did not crystallize, and quartz and braunite (Mn_7SiO_{12}; JCPDS No. 029–0890) were the only products obtained (Table 1). This probably occurred because the bulk composition of the starting mixture is close to the stability field of the manganese oxide (i.e., Mn_7SiO_{12}). Moreover starting materials solubility decreased with increasing contents of basic oxide such as MnO, making the nutrients closer to the composition of other phases (i.e. braunite).

As concern morphology, Mn-doped enstatite grew as prismatic crystals of different size (figure 3a, 3b, 3c) and with well-developed (100), (011), (010), (110), (0–11), (-1–10) and (1–10) faces. Based on the observation of crystals within a single run, crystals rarely grew showing intergrowths of single crystals parallel to the c-axis (figure 3c).

With regard to the size of the Mn-doped enstatite, it seems not to be related to the cooling rate. Indeed, crystals length were of about 8 mm both when the cooling rate was slower (1.7 °C/h; run EN7), and when it was faster (3.7 °C/h; run EN2). Conversely, an inverse correlation between size and amount of MnO dopant (wt%) has been observed; crystals size estimated by SEM images show a decreasing tendency with the increase in Mn concentration (see EN2 and EN8 in Table 1); average size of crystals was observed to increase at lower Mn content (6.76 wt%, run EN8) while at higher Mn content (14.52 wt%, run EN2), it is seen to decrease.

Probably, Mn acts as inhibitor of the growth: high amount of Mn atoms could hinder the diffusion of the nutrients decreasing the growth rate of the crystals during the reaction and resulting in crystals smaller in size [22].

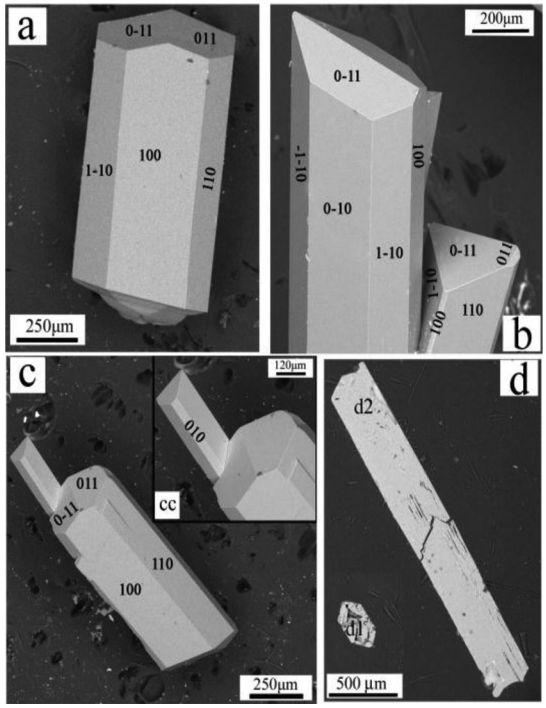

Fig. 3 Secondary electron SEM images of various Mn- doped enstatite crystals: (a) Mn-doped enstatite, run EN3; (b) Mn-doped enstatite, run EN1; (c) Mn-doped enstatite intergrowth, run EN3; (cc) magnification of c); (d) Transversal (d1) and longitudinal (d2) thin section of a single Mn-doped enstatite crystal, run EN1.

In regard to the chemical composition, quantitative analyses (EDS/SEM) carried out on 10 single crystals for each run, show that the chemical composition of Mn-doped enstatite was generally close to that of the starting materials, only for those with lower manganese content. However, a direct correlation was observed between Mn concentration in the starting mixture and Mn-dopant in the grown enstatite crystals even if the increase was not proportional to the amount of Mn present in the starting mixture. Indeed, we did not obtain $MnSiO_3$ when Mn was totally in substitution for Mg in the starting mixture (runs EN5, EN9). Probably the different characteristic of Mn^{2+} respect to the Mg^{2+} one may result in the deformation of the crystal structure, so it is not possible to obtain isomorphic series between enstatite $MgSiO_3$-$MnSiO_3$ at least under the experimental conditions of this study. The maximum amount of manganese indicated as MnO wt% reached 14.52 wt% (run EN8), thus the representative chemical formulae of Mn-doped enstatite is approximately $(Mg_{0.80}Mn_{0.20})SiO_3$ (Table1).

EDS/SEM chemical data showed that slow cooling (1.7 °C/h, EN6, EN7) favored the formation of enstatite with similar Mn dopant amount in each crystal

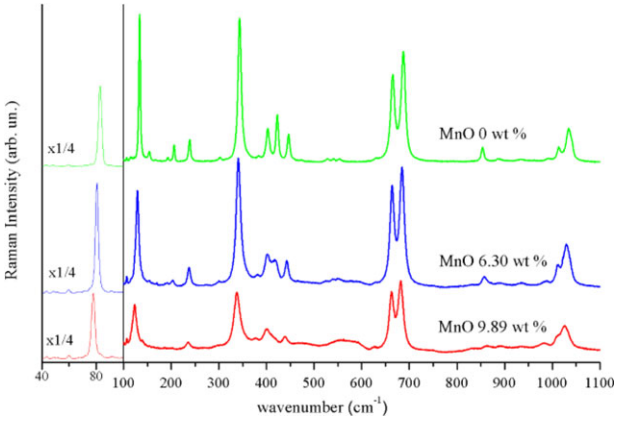

Fig. 4 Raman spectra of enstatite crystals with increasing amount of Mn doping, collected in parallel polarization (crystal axes zz) by using the 541.5 nm laser line for excitation. To improve the graphic clarity the low frequency part of spectra has been expanded in the wavenumber axis and reduced of a factor 4 in the intensity axis. All the scale are identical for the three spectra.

compared to those that were obtained from run with faster cooling rate (3.7 °C/h, EN1, EN3). Moreover, EDS/SEM analyses were also conducted on a thin section (figure 3d) of various single crystals from all runs to study the distribution of the dopant within the crystals. Mn-doped enstatite crystals from runs with faster cooling rate (3.7 °C/h) were slightly sector-zoned while the ones obtained from slower cooling (1.7 °C/h) had the same composition, indicating crystallization in equilibrium conditions. Probably growth rate controls the mechanism for sector-zoning formation [23]. The different starting temperature could influence only the concentration of the dopant in the melt (as it is known that impurities increase in the melt at higher temperatures), but not the diffusion and distribution of the dopant within the crystals which is more easily governed by the growth rate.

The total Raman spectrum of undoped enstatite ($MgSiO_3$) single crystal (run H1) was compared with Mn-doped enstatite spectra in order to study the spectral evolution at increasing Mn-doping content (figure 4).

For two different MnO dopant values, 6.30 wt% (run EN3) and 9.89 wt% (run EN8), the following trends in the Raman spectra were observed: i) a general down shifting of the peak frequency; ii) a broadening of the peaks. The peak-frequency shift of the strongest Raman active modes are shown in figure 5a. In particular the Raman band at about 686 cm^{-1} of the undoped enstatite spectrum, down-shifts to 680 cm^{-1} for 9.89 wt% Mn-doped compound (run EN8, figure 5a), in good agreement with the data reported by Stalder et al. [24] for Fe-doped enstatite. By the way the most relevant downshift is observed for the low frequency mode at 133 cm^{-1}, while all the other ones exhibit a lower downshift, of comparable amount (see figure 5a).

With regard to the linewidths, most of the Raman peaks show a remarkable broadening vs. the Mn-doping content. As shown in figure 5b this effect of the lattice disorder appears greater for the 134 and 343 cm^{-1} peaks. It is also interesting to remark that no appreciable linewidth increase is observed for the strongest and narrow peak at 83 cm^{-1}, which is, however, affected by frequency downshift vs. increasing Mn doping.

Similar phenomena of frequency downshift and broadening, although more difficult to measure and therefore not reported in figure 5, were also observed for other weaker Raman peaks occurring in the regions between 200 and 250 cm^{-1}, between 400 and 450 cm^{-1}, and at about 1000 cm^{-1} (see figure 4).

Figure 6 represents the CL emission spectra of undoped enstatite (run H1) and doped with increasing amount of Mn^{2+} (run EN3, 6.30%; run EN8, 9.89%).

At room temperature, no CL emission signal was obtained from undoped enstatite, while Mn-doped enstatite spectra are characterized by a broad red band emission located at 677 nm which intensity is directly proportional to Mn content (figure 6). The wavelength location of this red emission does not change with respect to that one resulting from nanometric Mn-doped enstatite synthesized by sol-gel method [11].

As confirmed by Lin Lin et al. [11] this broad band is attributed to the transition $^4T1g(G) \rightarrow {}^6A1g$ (S) of Mn^{2+} substitutional to Mg^{2+} position in enstatite [25]; the presence of one-dimensional chain of silica tetrahedra (SiO_4) in $MgSiO_3$ host favour this substitution respect to other more complex silicate structures [11]. The electronic transition $^4T1g(G) \rightarrow {}^6A1g(S)$ (responsible for luminescence in Mn^{2+} centers) is spin-forbidden and also Laporte forbidden for electric dipole transitions which accounts for the center of symmetry [26]. But the spin-forbiddenness is broken down to some extent by a small degree of spin-orbit coupling, while the Laporte-forbiddenness is broken by vibrational coupling of phonons with different parity [27]. For these reasons such transition is characterized by decay time of roughly 10 ms [28].

The energy of $^4T1g(G) \rightarrow {}^6A1g(S)$ Mn^{2+} transition strongly depends on symmetry and therefore on field strength [29]. In fact, according to the Mn^{2+} Tanabe–Sugano diagram, for octahedral coordination [30, 31], the 677 nm emission is due to the $^4T1g(G) \rightarrow {}^6A1g(S)$ Mn^{2+} transition for a crystal field parameter Δ near 10000 cm^{-1}.

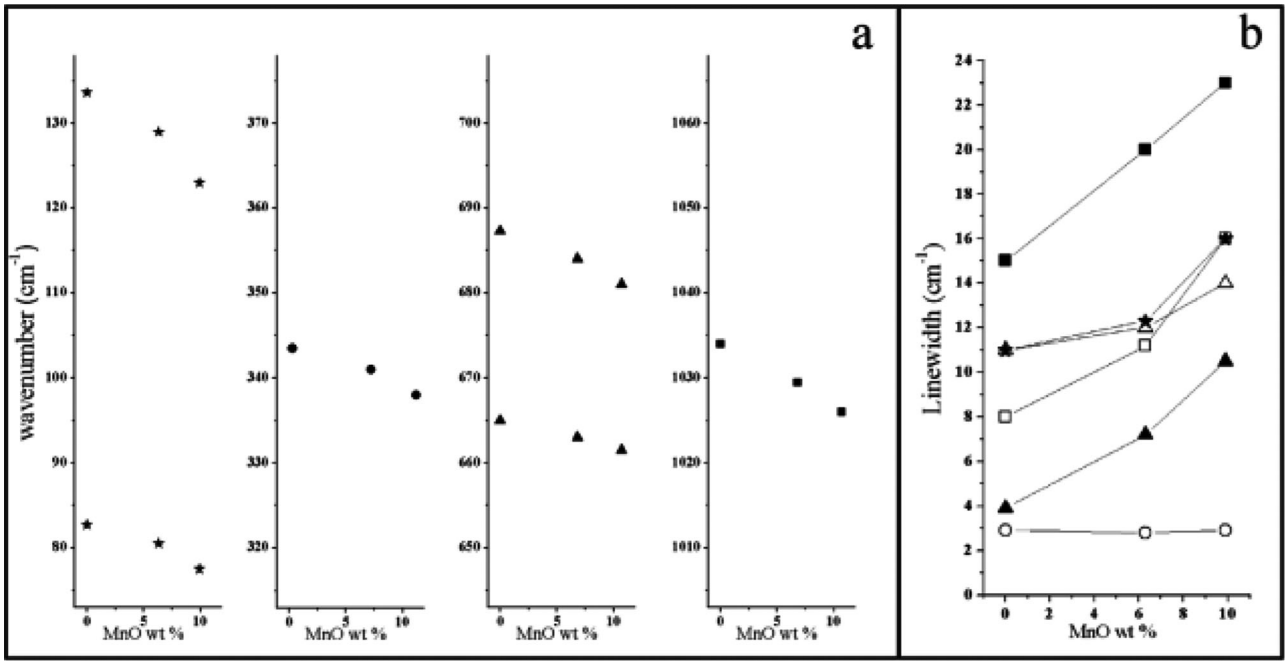

Fig. 5 (a) Frequencies of some Raman active modes of enstatite (the strongest) as a function of the Mn doping amounts; (b) linewidth of some Raman active modes of enstatite vs. the Mn doping amount. The following symbols correspond to the modes labelled after their wavenumber in the pure compound: open circles: 83 cm^{-1}; solid triangles: 134 cm^{-1}; open squares: 343 cm^{-1}; open triangles: 665 cm^{-1}; solid stars: 687 cm^{-1}; solid squares: 1034 cm^{-1}.

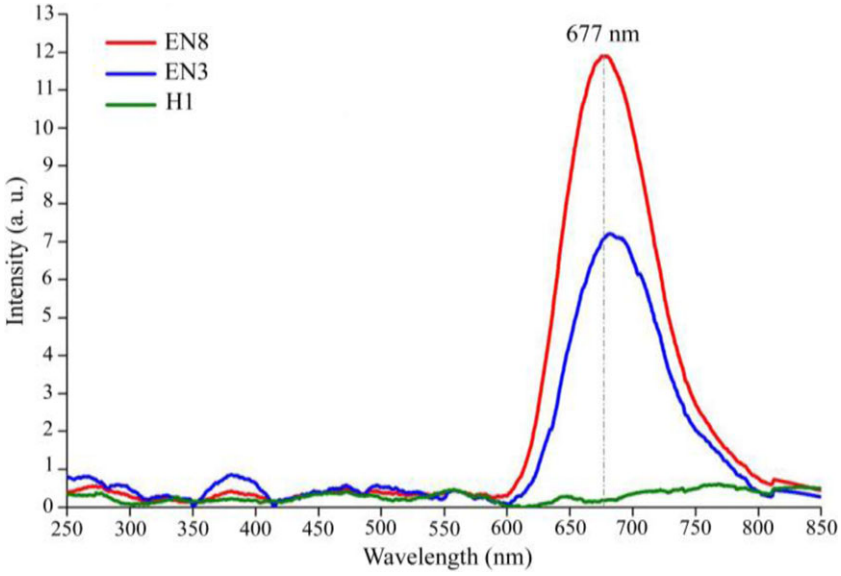

Fig. 6 Cathodoluminescence spectra of: undoped enstatite, run H1; Mn-doped enstatite with increasing amount of Mn^{2+} (run EN3, 6.30%; run EN8, 9.89%).

4 Conclusion

Enstatite single crystals doped with manganese were grown by the flux growth technique in the temperature range 600–1350 °C with lithium-vanadium-molybdate as melting agent.

The slow-cooling flux method is a good technique to obtain large and well-developed Mn-doped single enstatite crystals. The chemical composition of Mn-doped enstatite was generally close to that of the starting materials only for those with lower manganese content. However, under the experimental conditions of this study,

enstatite was not obtained when Mg was totally substituted by manganese in the starting mixture. An increase of Mn content in the enstatite crystals produces a decrease in their size. The best conditions for producing enstatite crystals with high crystallinity, homogeneous distribution of manganese and with the highest content of manganese occur by slow cooling to 650 °C from 1050 °C of a suitable starting mixture, at a cooling rate of 1.7 °C/h.

The Raman line shapes continuously change with increasing of Mn-doping amount in enstatite. The observed changes reflect the modifications in local arrangements induced by the increase of manganese in the crystals structure. Cathodoluminescence spectrum of enstatite was strongly affected by Mn^{2+} cations showing a strong red band emission located at 677 nm. Mn-doped enstatite could be suitable for a red-light emitting phosphor and as microwave and millimeterwave materials.

Key words. growth from melt, single crystals, Mn-doped enstatite, characterization.

References

[1] G. H. Beall, Ceram. Trans. **30**, 241 (1993).
[2] W. Holand and G. N. Beall, Glass-Ceramic Technology (The American Ceramic Society, Westervillee, OH, 2002).
[3] M. E. Song, J. S. Kim, M. R. Joung, S. Nahmw, Y. S. Kim, J. H. Paik, and B. H. Choi, J. Am. Ceram. Soc. **91**, 2747 (2008).
[4] G. N. Sun and E. S. Kim, Ferroelectrics. **434**, 44 (2012).
[5] H. Ohsato, Seramikkusu. **39**, 578 (2004).
[6] J. R. Smyth and J. To, Am. Mineral. **62**, 1252 (1977).
[7] E. Cavalli and M. Bettinelli, Opt. Mater. **2**, 151 (1993).
[8] R. Moncorgè, M. Bettinelli, Y. Guyot, E. Cavalli, J. A. Capobanco, and S. Girard, J. Phys. Condens. Matter. **11**, 6831 (1999).
[9] A. Bloise, V. Pingitore, D. Miriello, C. Apollaro, D. Armetano, E. Barrese, and A. Oliva, J. Cryst. Growth. **329**, 86 (2011).
[10] H. Kanazawa, K. Ito, H. Sato, M. Kumatoriya, K. Miyazaki, S. Uehara, H. Tsuda, K. Kuzawa, N. Kawame, T. Kitazawa, O. Tamada, M. B. Boisen Jr., and H. Takei, J. Cryst. Growth. **30**, 492 (2007).
[11] L. Lin, Y. Min, S. Chaoshu, Z. Weiping, and Y. Baogui, J. Rare Earth. **24**, 104 (2006).
[12] L. Lin, S. Chaoshu, W. Zhifang, Z. Weiping, and M. Yin, J. Alloy. Compd. **466**, 546 (2008).
[13] J. Ito, Geophys. Res. Lett. **2**, 533 (1975).
[14] A. Bloise, E. Belluso, E. Barrese, D. Miriello, and C. Apollaro, Cryst. Res. Technol. **44**, 590 (2009).
[15] M. Ozima, J. Jpn, Assoc. Mineral. Petrol. Econ. Geol. **3**(Suppl.), 97 (1982).
[16] J. Ito, Geophys. Res. Lett. **2**, 533 (1982).
[17] A. Bloise, E. Barrese, C. Apollaro, and D. Miriello, Cryst. Res. Technol. **44**, 463 (2009).
[18] T. Tanaka and H. Takey, J. Cryst. Growth. **180**, 206 (1997).
[19] R. S. Coe and S. H. Kirby, Contrib. Mineral. Petrol. **52**, 29 (1975).
[20] S. H. Kirby and M. A. Etheridge, Phys. Chem. Minerals. **7**, 105 (1981).
[21] M. Ushio, N. Kobayashi, M. Suzuki, and Y. Sumiyoshi, J. Am. Ceram. Soc. **75**, 1554 (1991).
[22] K. Sangwal, Prog. Crystal Growth Charact. **32**, 3 (1996).
[23] S. C. Schwandt and G. A. Mckay, Am Mineral **91**, 1607 (2006).
[24] R. Stalder, A. Kronz, and B. C. Schmidt, Eur. J. Mineral. **21**, 27 (2009).
[25] M. Gaft, R. Reisfeld, and G. Panczer, Modern Luminescence Spectroscopy of Minerals and Materials (Springer, Berlin Heidelberg, 2005).
[26] G. Walker, Mineralogical Mag. **53**, 201 (1989).
[27] G. Walker, in: Chemical Bonding and Spectroscopy in Mineral Chemistry, edited by F. J. Berry and D. J. Vaughan (Chapman & Hall, London, 1985), p. 103.
[28] G. Blasse and B. C. Grabmaier, Luminescent Materials (Springer-Verlag, Heidelberg, Berlin, 1994).
[29] H. Keppler, Am. Mineral. **77**, 62 (1992).
[30] Y. Tanabe and S. Sugano, J. Phys. Soc. Jpn. **9**, 753 (1954).
[31] Y. Tanabe and S. Sugano, J. Phys. Soc. Jpn. **9**, 766 (1954).

